

## RESEARCH ARTICLE

# The focal adhesion targeting domain of p130Cas confers a mechanosensing function

Peta M. Bradbury<sup>1,2</sup>, Kylie Turner<sup>1</sup>, Camilla Mitchell<sup>1</sup>, Kaitlyn R. Griffin<sup>1</sup>, Shiloh Middlemiss<sup>1</sup>, Loretta Lau<sup>1</sup>, Rebecca Dagg<sup>1</sup>, Elena Taran<sup>3</sup>, Justin Cooper-White<sup>4</sup>, Ben Fabry<sup>5</sup> and Geraldine M. O'Neill<sup>1,2,\*</sup>

## ABSTRACT

Members of the Cas family of focal adhesion proteins contain a highly conserved C-terminal focal adhesion targeting (FAT) domain. To determine the role of the FAT domain in these proteins, we compared wild-type exogenous NEDD9 with a hybrid construct in which the NEDD9 FAT domain had been exchanged for the p130Cas (also known as BCAR1) FAT domain. Fluorescence recovery after photobleaching (FRAP) revealed significantly slowed exchange of the fusion protein at focal adhesions and significantly slower two-dimensional migration. No differences were detected in cell stiffness as measured using atomic force microscopy (AFM) and in cell adhesion forces measured with a magnetic tweezer device. Thus, the slowed migration was not due to changes in cell stiffness or adhesion strength. Analysis of cell migration on surfaces of increasing rigidity revealed a striking reduction of cell motility in cells expressing the p130Cas FAT domain. The p130Cas FAT domain induced rigidity-dependent phosphorylation of tyrosine residues within NEDD9. This in turn reduced post-translational cleavage of NEDD9, which we show inhibits NEDD9-induced migration. Collectively, our data therefore suggest that the p130Cas FAT domain uniquely confers a mechanosensing function.

**KEY WORDS:** Focal adhesion, Mechanosensing, NEDD9, P130Cas, FAT, Cell migration

## INTRODUCTION

Focal adhesions sense biochemical and mechanical features of the extracellular environment and transmit this information to the cell. The Cas-family proteins NEDD9 (also known as HEF1 and Cas-L) and p130Cas (also known as BCAR1) are examples of signalling proteins that are recruited to focal adhesions, where they regulate cell migration signals (Cary et al., 1998; Klemke et al., 1998; Fashena et al., 2002; Natarajan et al., 2006; Meenderink et al., 2010; Kong et al., 2011; Baquiran et al., 2013; Bradbury et al., 2014). Both proteins contain a C-terminal focal adhesion targeting (FAT) domain (Arold et al., 2002; Mace et al., 2011), characterised by extensive primary sequence and tertiary structural similarity. The identification of the FAT domain module in functionally

diverse focal adhesion-associated proteins (Arold et al., 2002; Schmalzigaug et al., 2007; Garron et al., 2009; Mace et al., 2011) suggests the domain has an important role in focal adhesion biology. First described in focal adhesion kinase (FAK) (Arold et al., 2002; Hayashi et al., 2002), the compact four-helix bundle FAT domain was subsequently identified in the Cas-family of proteins (Arold et al., 2002; Garron et al., 2009; Mace et al., 2011), in the focal adhesion protein vinculin (Arold et al., 2002), in G protein-coupled receptor kinase-interacting protein ArfGAP 1 (GIT1) (Schmalzigaug et al., 2007) and more recently in cerebral cavernous malformation protein 3 (CCM3) (Li et al., 2010). The FAT domain mediates FAK interaction with paxillin (Hayashi et al., 2002; Hoellerer et al., 2003), FAK intra-molecular interactions (Brami-Cherrier et al., 2014), CCM3 interaction with CCM2 (Draheim et al., 2015), and interactions between the Cas-family proteins and members of the SH2-containing protein (NSP) family – NSP1, NSP2 (also known as AND-34 and BCAR3) and NSP3 (also known as SHEP1 and CHAT) (Garron et al., 2009; Mace et al., 2011).

Contrasting with the primarily pro-migratory function ascribed to p130Cas (Tikhmyanova et al., 2010), NEDD9 function in cell migration is context specific; in some cell backgrounds, NEDD9 is pro-migratory (Ohashi et al., 1998; van Seventer et al., 2001; Kim et al., 2006; Natarajan et al., 2006; Bui et al., 2009; Izumchenko et al., 2009; Lucas et al., 2010; Kong et al., 2011), in others, NEDD9 restrains cell migration (Simpson et al., 2008; Seo et al., 2011; Zhong et al., 2012). This divergent function suggests that NEDD9 may tune the focal adhesion response depending on the tissue and cellular context. Notably, NEDD9 is expressed in a restricted repertoire of tissues relative to p130Cas (O'Neill et al., 2000), which is ubiquitously expressed, pointing to a probable tissue-specific function for NEDD9. In mouse embryo fibroblasts (MEFs), phosphorylation slows NEDD9 molecular exchange at focal adhesions, reduces focal adhesion dynamics and, hence, decelerates cell migration (Baquiran et al., 2013; Bradbury et al., 2014). Phosphorylation-mediated interactions with other molecules that are resident at the focal adhesions stabilise NEDD9 interactions at the focal adhesions (Bradbury et al., 2014).

NEDD9 and p130Cas have a conserved protein–protein interaction domain structure (O'Neill et al., 2000), comprising an N-terminal SH3 domain, followed by a substrate binding domain (SD) with multiple consensus tyrosine phosphorylation sites. A serine-rich region follows the SD, and lastly the FAT domain, also known as the Cas-family C-terminal homology (CCH) domain (Donato et al., 2010). The NEDD9 sequence also encompasses a protease cleavage site, DLVD, that when cleaved releases an N-terminal 55 kDa peptide (Law et al., 1998). The N-terminal SH3 and C-terminal FAT domains of NEDD9 and p130Cas each contribute to focal adhesion targeting (Harte et al., 1996; Nakamoto et al., 1997; O'Neill and Golemis, 2001; Donato et al., 2010; Bradbury et al., 2014). Upstream of the FAT domain, both proteins

<sup>1</sup>Children's Cancer Research Unit, Kids Research Institute, The Children's Hospital at Westmead, Westmead, New South Wales 2145, Australia. <sup>2</sup>Discipline of Paediatrics and Child Health, The University of Sydney, Sydney, New South Wales 2000, Australia. <sup>3</sup>Australian National Fabrication Facility-Queensland node, Australian Institute for Bioengineering and Nanotechnology, University of Queensland, St. Lucia, Queensland 4067, Australia. <sup>4</sup>Tissue Engineering and Microfluidics Laboratory, Australian Institute for Bioengineering and Nanotechnology, University of Queensland, St. Lucia, Queensland 4067, Australia. <sup>5</sup>Department of Physics, Friedrich-Alexander University of Erlangen-Nuremberg, 91054 Erlangen, Germany.

\*Author for correspondence (geraldine.oneill@health.nsw.gov.au)

contain a consensus binding site for Src-family kinases (O'Neill et al., 2000). FAK phosphorylates the Src-binding site leading to Src docking (Ruest et al., 2001). Subsequently, Src phosphorylates tyrosine residues in the SD, creating binding sites for downstream mediators, such as the adaptor protein Crk. Phosphorylation is regulated by integrin receptor ligation and focal adhesion formation, and this reduces NEDD9 cleavage at the DLVD site (O'Neill and Golemis, 2001). Previous studies have shown that p130Cas is a mechanosensor at focal adhesions given that force applied to the p130Cas SD leads to increased phosphorylation (Sawada et al., 2006; Mui et al., 2015). This stretch activation requires tethering at either end of the p130Cas SD. While the N-terminal SH3 domain has been implicated in p130Cas mechanosensing (Janošiak et al., 2014b), the requirement for the FAT domain is unknown. As the FAT domain is an important molecular tether at focal adhesions, it may also play a role in mechanosensing.

In the present study, we sought to understand the role of the FAT domain in Cas-family proteins by analysing fusion proteins in which the NEDD9 FAT domain was exchanged for the homologous p130Cas FAT domain. Our data reveal that the p130Cas FAT domain confers a mechanosensory function; evidenced by an inversion of the relationship between substrate rigidity and cell speed compared to that of cells expressing wild-type NEDD9.

## RESULTS

### Exchanging the NEDD9 FAT domain

The NEDD9 C-terminal domain, originating at residue 695, constitutes the minimal FAT domain (Garron et al., 2009) (Fig. 1A). Reports that the C-terminal FAT domains of p130Cas and NEDD9 show high sequence similarity (Arold et al., 2002; Singh et al., 2008; Garron et al., 2009; Mace et al., 2011) were confirmed by comparison of orthologous NEDD9 and p130Cas FAT domains from human, mouse, rat and chicken. Sequence alignments indicate a high level of conservation (Fig. 1B), with amino acid residues coloured in orange/red tones indicating the highest sequence conservation (note that the corresponding FAT domain in human p130Cas begins at residue 731). As the NEDD9 FAT domain induces cell rounding and apoptosis when expressed in isolation (O'Neill and Golemis, 2001), it is not possible to compare NEDD9 and p130Cas FAT domain function in cell migration through analysis of the discrete FAT domains as peptides. Therefore, we created an expression construct in which the NEDD9 FAT domain was exchanged for the p130Cas FAT domain (Fig. 2A; NEDD9::CasFAT). Note that the difference in p130Cas amino acid residue numbering in Fig. 2A versus those shown in Fig. 1B, reflects that the sequence used to create the NEDD9::CasFAT fusion was derived from the rat p130Cas sequence as opposed to the human sequence indicated in Fig. 1A. The resulting NEDD9::CasFAT construct retains the upstream wild-type NEDD9 sequence, including the Src kinase-binding motif (DYDY) and the DLVD cleavage site. GFP-tagged NEDD9 wild-type and NEDD9::CasFAT fusion proteins were expressed in A172 glioblastoma cells engineered to express tetracycline-inducible shRNA targeting NEDD9. The fusion protein expression constructs carried mutations in the NEDD9 shRNA-targeting sequence to allow expression following depletion of endogenous NEDD9. As shown, tetracycline addition efficiently depleted the endogenous NEDD9 protein doublet (Fig. 2B, long exposure). Further, the NEDD9 wild type and NEDD9::CasFAT rescue constructs were expressed in the presence of tetracycline (Fig. 2B,C). Both fusion proteins displayed the expected NEDD9 doublet, corresponding to the endogenous protein phosphorylated

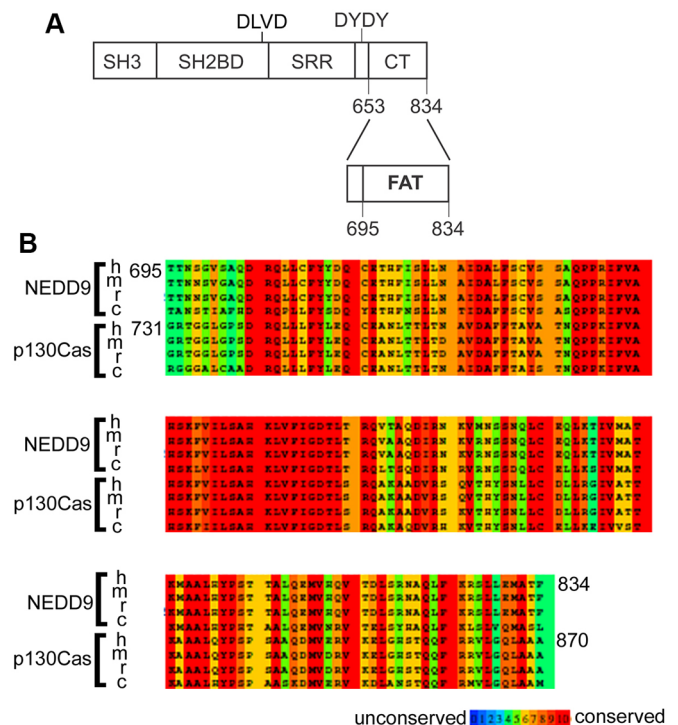


**Fig. 1. NEDD9 domain structure and p130Cas protein FAT domain alignment.** (A) Schematic representation of the NEDD9 protein sequence showing the N-terminal SH3 domain, followed by the SH2-binding domain (SH2BD), serine-rich region (SRR) and the C-terminal domain (CT) containing the Src kinase-binding site (DYDY). Also shown is the cleavage site (DLVD); post-translational cleavage at this site generates a 55 kDa N-terminal peptide. The extracted region indicates the position of the focal adhesion-targeting (FAT) domain comprising residues 695–834 in the CT. (B) NEDD9 and p130Cas FAT (CasFAT) domains aligned using the PRALINE website. Amino acid residue numbers for human NEDD9 and p130Cas are shown. Sequences correspond to human (h), mouse (m), rat (r) and chicken (c). Colours indicate sequence conservation, with red indicating the most conserved alignment position and blue denoting the least conserved alignment position.

forms (Law et al., 1998). We further determined that neither NEDD9 depletion (Fig. 2D) nor exogenous protein expression (Fig. 2E) altered endogenous levels of the interacting partner protein FAK or p130Cas. Quantification by performing densitometry confirmed that there were no significant changes to FAK or p130Cas expression (Fig. 2F).

### CasFAT retains focal adhesion targeting information but slows molecular exchange

The FAT domain is required to target NEDD9 to focal adhesions (O'Neill and Golemis, 2001; Bradbury et al., 2014); therefore, we investigated whether CasFAT was competent to target the fusion protein to focal adhesions. Immunofluorescence analysis revealed that CasFAT indeed substitutes for the NEDD9 FAT domain in targeting the molecule to focal adhesions (Fig. 3A). Comparison of the morphology of paxillin-positive focal adhesions showed that cells expressing GFP-tagged wild-type NEDD9 and NEDD9::CasFAT had the same number and size of focal adhesions (Fig. 3B). The size of individual focal adhesions was also unchanged (GFP–NEDD9=12.2 pixel±0.5; GFP–NEDD9::CasFAT=12.2 pixel±0.6; mean±s.e.m.; not significant, Student's *t*-test). Thus, focal adhesion morphologies were unaffected by the CasFAT substitution. Since NEDD9 constructs lacking the FAT domain show rapid molecular exchange at focal adhesions when compared with full length

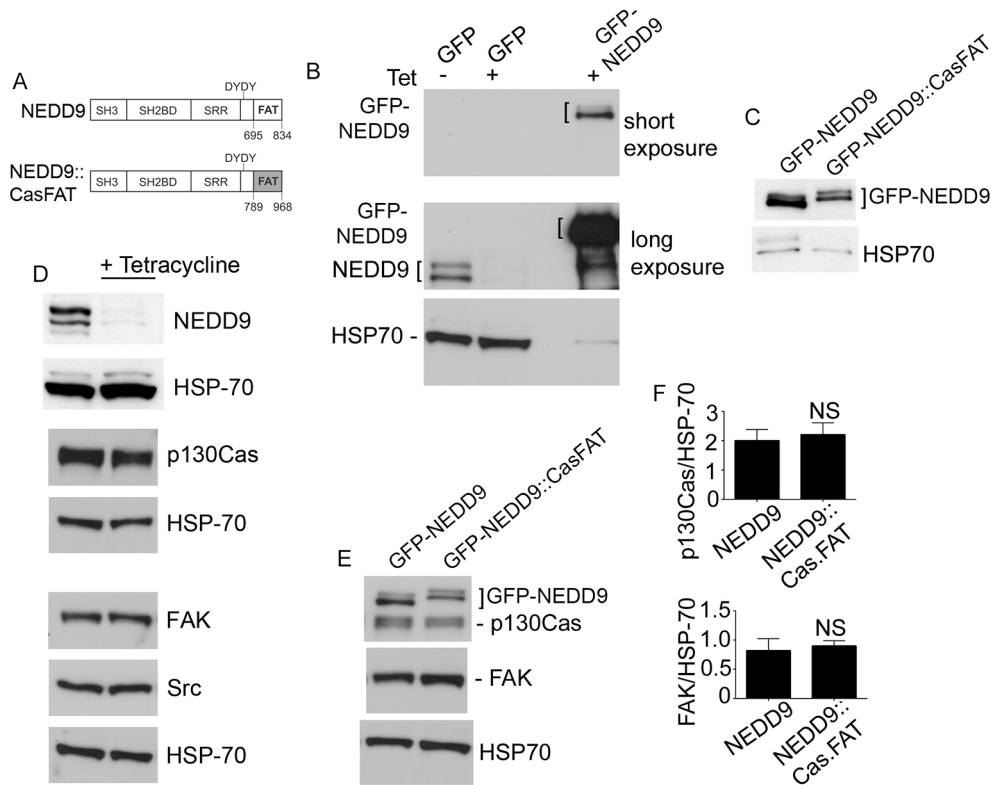


**Fig. 2. Tetracycline-inducible NEDD9 knockdown and FAT domain fusion protein expression.** (A) Schematic representation of the NEDD9 p130Cas FAT domain exchange construct. The FAT domain of NEDD9 (residues 695–834) was replaced with p130Cas residues 789–968 to generate NEDD9::CasFAT. (B) Western blot analysis of whole cell lysates of control cells (Tet–) or following NEDD9 depletion (Tet+) that had been transfected with GFP vector control or the GFP-tagged NEDD9 rescue construct. Note the doublets of NEDD9 protein corresponding to the 105 kDa and 115 kDa NEDD9 phosphorylated forms (Bradshaw et al., 2011) fused to GFP. Two different autoradiograph exposures are shown to reveal the doublet of the GFP-tagged NEDD9 protein (short exposure) and endogenous NEDD9 (long exposure). (C) Western blots showing exogenous GFP-tagged wild-type NEDD9 and NEDD9::CasFAT expression following endogenous NEDD9 depletion. Note that the images shown are from an exposure following antibody probing for both NEDD9 and HSP70. The same blot is reshown in Fig. 7C. (D) Endogenous p130Cas, FAK and Src expression under control conditions and following NEDD9 depletion (+Tetracycline). (E) Endogenous p130Cas and FAK expression following exogenous expression of GFP–NEDD9 and GFP–NEDD9::CasFAT in the presence of tetracycline to deplete endogenous NEDD9. Note that the p130Cas antibody-binding epitope is conserved in the sequence of NEDD9 and is located upstream of the FAT domain (Law et al., 1998), therefore p130Cas antibodies detect both endogenous p130Cas and the exogenously expressed GFP fusion proteins. HSP70 expression is shown for all blots to indicate protein loading. (F) Histograms showing densitometry measurements of the levels of p130Cas and FAK expressed relative to those of HSP70 in cells that had been transfected with the indicated constructs. Data represent the average of triplicate repeats on separate days and error bars show the s.e.m. NS, not significant; Student's *t*-test.

NEDD9 (Bradbury et al., 2014), we determined the effect of the FAT domain on the rates of protein exchange. Fluorescence recovery after photobleaching (FRAP) analysis of GFP-positive focal adhesions revealed that GFP–NEDD9::CasFAT fluorescence was significantly slower to recover than that of the wild-type NEDD9 molecule (Fig. 3C–E).

### CasFAT specifically inhibits cell migration

Next, we questioned the effects on cell speed. Previous demonstrations of cell-type-specific effects (Ohashi et al., 1998; van Seventer et al., 2001; Kim et al., 2006; Natarajan et al., 2006; Simpson et al., 2008; Bui et al., 2009; Izumchenko et al., 2009; Lucas et al., 2010; Kong et al., 2011; Seo et al., 2011; Zhong et al., 2012) first necessitated the assessment of NEDD9 expression and the regulation of A172 cell speeds. Time-lapse imaging, tracking and quantification of the mean squared displacement (MSD) revealed that NEDD9 depletion significantly increased A172 two-dimensional (2D) migration speeds (Fig. 4A,B). Exogenous expression of the NEDD9 rescue construct returned migration speeds to those seen under control conditions, confirming that the effect was NEDD9-dependent

(Fig. 4A,B). These findings parallel earlier data showing increased 2D migration speeds of NEDD9-knockout MEFs (Zhong et al., 2012). Previously, we have shown that NEDD9-knockout MEFs exhibit increased surface expression of the fibronectin receptor integrin  $\alpha 5\beta 1$  (Zhong et al., 2012). However, analysis of A172 adhesion to fibronectin, and to other extracellular matrix components, revealed no difference in adhesion following NEDD9 depletion (Fig. 4C). Correspondingly, the surface expression of integrin  $\alpha 5\beta 1$  was unchanged following NEDD9 depletion in the A172 cells (Fig. 4C, inset); thus, this effect may be cell-type specific. Previous studies have reported that loss of FAK or p130Cas from focal adhesions decreases intracellular stiffness (Bae et al., 2014; Janoštiak et al., 2014b). Consequently, we assessed membrane compliance by performing AFM; however, there was no significant difference in Young's modulus between control cells and NEDD9-depleted cells (Fig. 4D). Collectively, these data reveal that NEDD9 restrains 2D migration of A172 cells but that this is not due to changes in adhesion or cell compliance.

We next questioned the effect of CasFAT on cell speed. Strikingly, NEDD9::CasFAT-expressing cells were significantly

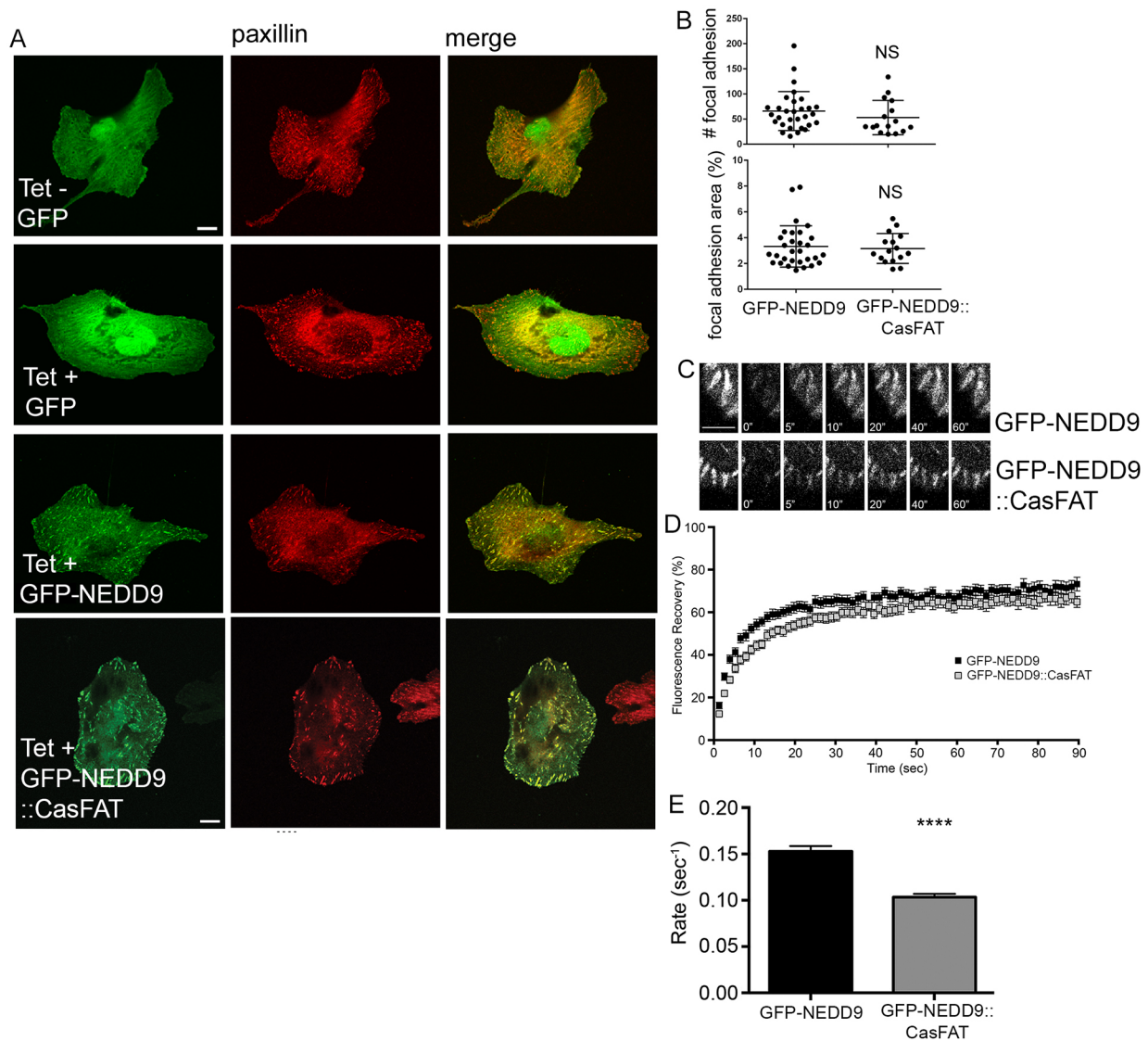


**Fig. 3. CasFAT slows dynamic exchange at focal adhesions.** (A) Confocal images of control cells (Tet<sup>-</sup>) or following NEDD9 depletion (Tet<sup>+</sup>) and transfection with GFP vector control, GFP-NEDD9 or GFP-NEDD9::CasFAT, as indicated. Shown are single confocal slices for GFP, paxillin and merged images. Scale bars: 20  $\mu$ m. (B) The mean number of paxillin-positive focal adhesions per cell (top graph) and the paxillin-positive focal adhesion area expressed as a percentage of the total cell area (bottom graph) in cells expressing GFP-NEDD9 and GFP-NEDD9::CasFAT, as indicated. Data points represent the mean value for each cell ( $\geq 17$  transfected cells examined per construct). NS, not significant; Student's *t*-test. (C) Representative images of focal adhesions before photobleaching (first panels), immediately post bleaching (0", 0 s) and throughout fluorescence recovery (5–60"). Scale bars: 5  $\mu$ m. (D) Recovery kinetics of GFP-NEDD9 (black squares) and GFP-NEDD9::CasFAT (grey squares). Data show normalised average fluorescence recovery over the 90 s recovery period. (E) Mean fluorescence recovery rate under the indicated conditions. \*\*\*\**P*>0.0001; Student's *t*-test. Data represent pooled means of  $n \geq 4$  independent experiments ( $\geq 49$  total focal adhesions analysed per construct). Data are mean  $\pm$  s.e.m.

slower than cells under all other conditions tested (Fig. 5A). In fact, the majority of NEDD9::CasFAT cells were non-motile (Fig. 5B). To determine whether the effects on cell speed are specific to the expression of CasFAT, we analysed an alternative chimeric protein in which the NEDD9 FAT domain was substituted with the FAT domain of FAK (NEDD9::FAKFAT). Importantly, this chimeric protein also targeted to focal adhesions (Fig. 5C,D). FRAP analysis of NEDD9::FAKFAT revealed that the FAK FAT domain significantly slowed molecular exchange at focal adhesions (Fig. 5E), similar to the results seen with the NEDD9::CasFAT protein. But in contrast to NEDD9::CasFAT-expressing cells, cells expressing NEDD9::FAKFAT migrated with the same speed as wild-type NEDD9-expressing cells and significantly faster than

NEDD9::CasFAT-expressing cells (Fig. 5A). This indicates that the slowing of cell migration speed through expression of the NEDD9::CasFAT molecule is not simply a result of slowed molecular exchange at the focal adhesions. We tested whether the slowed migration speeds correlated with increased adhesive force, thereby anchoring cells and preventing migration. Using a magnetic tweezer device, we analysed cell adhesion force to fibronectin-coated magnetic beads exposed to increasing lateral pulling force in the range of 0 to 40 nN. This revealed no significant difference in adhesive force between control cells and NEDD9-depleted cells versus the cells expressing GFP-NEDD9::CasFAT (Fig. 5F). Therefore, CasFAT arrests cell migration but does not change the adhesive force.

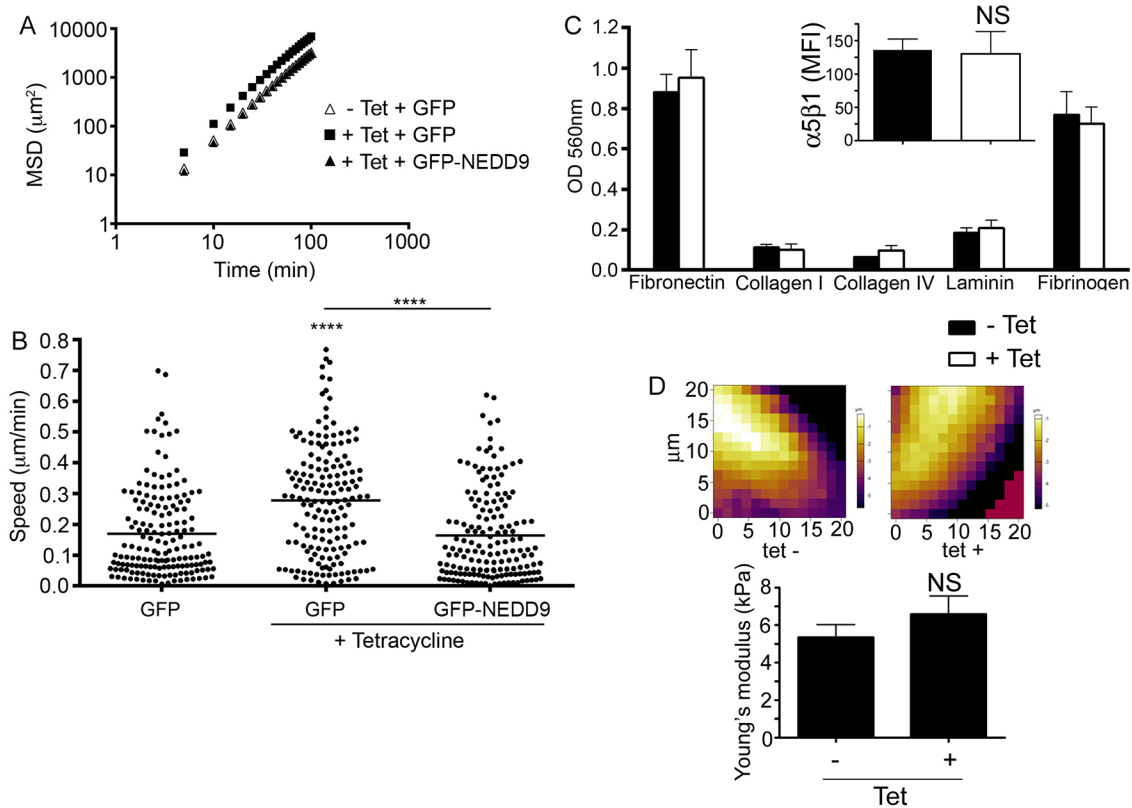


**Fig. 4. Exogenous NEDD9 rescues the faster migration induced by NEDD9 knockdown.** (A) MSD calculated from trajectories of control cells (–Tet) transfected with GFP vector (white triangles); following endogenous NEDD9 depletion (+Tet) and transfection with GFP vector (black squares); and following endogenous NEDD9 depletion and expressing GFP–NEDD9 (black triangles). (B) Speeds of individual cells grown under the conditions described in A. Data represent pooled means of  $n \geq 155$  total cells analysed per construct. \*\*\*\* $P < 0.0001$ , one-way ANOVA with Tukey's multiple comparison post-test. (C) Adhesion to the indicated matrices was measured in control cells (–Tet) and following NEDD9 depletion (+Tet). No statistical difference in adhesion to any matrix was seen between either condition; NS, not significant; Student's *t*-test. Data represent pooled averages of three independent experiments. Inset graph shows surface expression [mean fluorescence intensity (MFI) of  $\alpha 5\beta 1$  integrin receptor by FACs analysis]. NS, not significant; Student's *t*-test. (D) AFM height maps of a control A172 cell (left) and following NEDD9 knockdown (Tet+, right image) were generated for measurements of Young's moduli. Bar plot shows mean  $\pm$  s.e.m. of  $n > 11$  individual cells from three separate experiments analysed per condition, with 4–16 measurements performed per cell. NS, not significant; Student's *t*-test. Data shown are mean  $\pm$  s.e.m.

### Matrix rigidity enhances CasFAT-mediated inhibition of migration

Based on previous observations that p130Cas is a mechanotransducing protein (Sawada et al., 2006; Mui et al., 2015), we questioned whether the CasFAT confers sensitivity to rigidity. To address this, we analysed migration on soft fibronectin-coated polyacrylamide (PAM) hydrogels of 0.2 kPa and 1.0 kPa. Cells expressing either GFP–NEDD9 or GFP–NEDD9::CasFAT exhibited a rounded appearance on the softest gels and a more elongated appearance on 1.0 kPa gels (Fig. 6A). NEDD9 depletion caused cells to move faster than control cells, both on the 0.2 kPa and 1.0 kPa gels, as well as on the plastic dishes (Fig. 6B). Importantly, exogenous NEDD9 expression reversed the effects of NEDD9 depletion (Fig. 6B). Contrasting this rigidity-dependent induction of speed, cells expressing the NEDD9::CasFAT construct moved fastest on the 0.2 kPa gels, while migration was significantly inhibited on the 1.0 kPa gels and plastic surface (Fig. 6B). Paralleling this finding, the percentage of motile NEDD9::CasFAT cells significantly decreased with increasing substrate rigidity, but cells expressing wild-type NEDD9 were unaffected (Fig. 6C). The rigidity-dependent effect appears to be specific to CasFAT as cells expressing NEDD9::FAKFA did not slow with increased rigidity and instead exhibited the same response as cells expressing NEDD9 (Fig. 6B). Importantly, there was no difference

in polarity between cells expressing either GFP–NEDD9 or GFP–NEDD9::CasFAT when compared between cells grown on substrates of the same rigidity (Fig. 6D). Furthermore, there was no difference in the directional persistence (ratio of the vectorial distance traveled to the total path length described by the cell) between cells expressing GFP–NEDD9 versus those expressing GFP–NEDD9::CasFAT (ratio values of  $0.3 \pm 0.015$  versus  $0.30 \pm 0.017$ ; mean  $\pm$  s.e.m.; not significant, Student's *t*-test) during migration on plastic. Therefore, these data suggest that CasFAT-mediated reductions in cell migration are unlikely to be due to altered polarity. Collectively, these data suggest that CasFAT plays an important role in sensing external mechanical force.

### CasFAT induces rigidity-dependent NEDD9 phosphorylation and inhibits cleavage

The application of external force to p130Cas stretches the molecule and activates its signalling function through enhanced phosphorylation of the substrate-binding domain (Sawada et al., 2006). We therefore next assessed if CasFAT increased NEDD9 tyrosine phosphorylation. Our analyses confirmed that phosphorylation of tyrosine residues within NEDD9::CasFAT was 1.7-fold greater than that of the wild-type NEDD9 protein (Fig. 7A). Expression levels of NEDD9::CasFAT were consistently low, which agrees with previous demonstrations that phosphorylation of

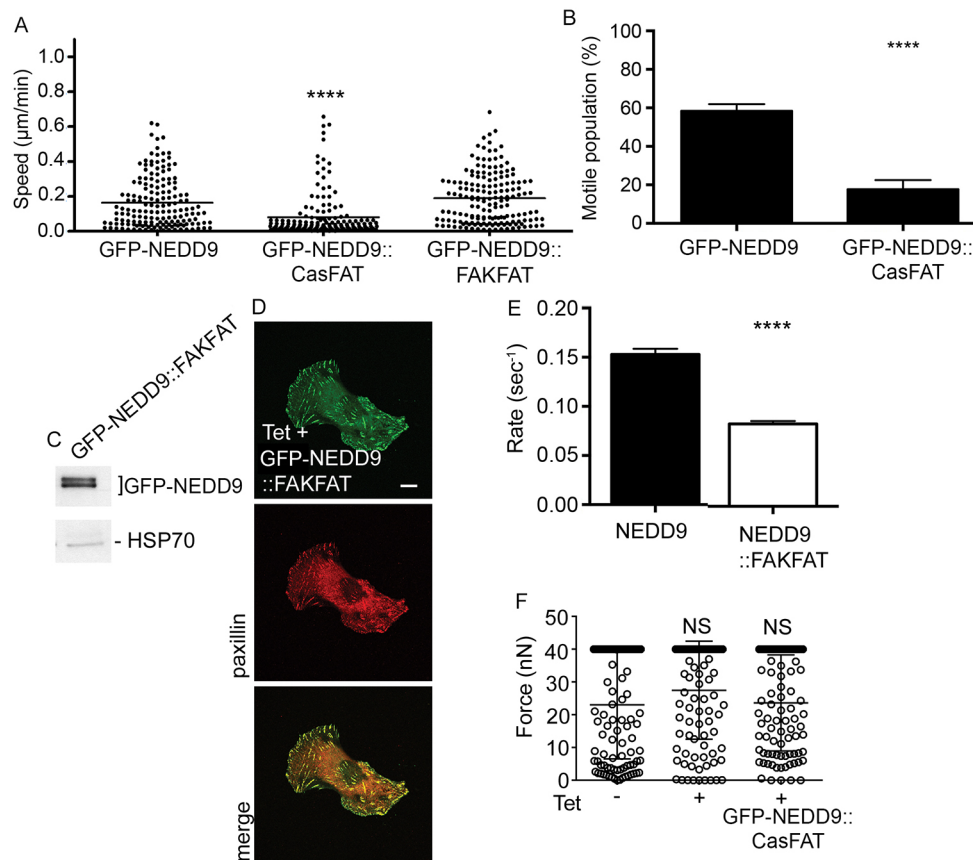


**Fig. 5. Comparison of CasFAT and FAKFAT domain effects.** (A) Speeds of individual A172 cells following depletion of endogenous NEDD9 and transfection with the indicated constructs. Note that the GFP–NEDD9 data are the same as that shown in Fig. 4B, replicated here for comparison. \*\*\*\* $P < 0.0001$  compared to GFP–NEDD9, Student's *t*-test.  $n \geq 163$  total cells analysed per construct. (B) The percentage of motile cells under the indicated conditions. Data represent pooled means of  $n \geq 4$  independent experiments ( $\geq 163$  individual cells analysed per construct). \*\*\*\* $P < 0.0001$ , Student's *t*-test. (C) Western blot showing expression of the GFP–NEDD9::FAKFAT chimeric protein. (D) Confocal images of cells following NEDD9 depletion (Tet+) and transfection with GFP–NEDD9::FAKFAT. Shown are single confocal slices for GFP, paxillin and merged images. Scale bar: 20  $\mu\text{m}$ . (E) Mean fluorescent recovery rate of GFP–NEDD9::FAKFAT under the indicated conditions. \*\*\*\* $P > 0.0001$ , Student's *t*-test. Data represent pooled means of  $n \geq 4$  independent experiments ( $\geq 49$  total focal adhesions analysed per construct). Note that the GFP–NEDD9 data is the same as that shown in Fig. 3E, replicated here for comparison. (F) Measurement of force at which fibronectin-coated magnetic beads could be detached from the cell surface following application of a linearly increasing force with a magnetic tweezer device. Circles represent individual cell measurements. NS, not significant, one-way ANOVA. Data shown are means  $\pm$  s.e.m.

NEDD9 regulates its proteasomal degradation (Liu et al., 2000). Treatment with the phosphatase inhibitor  $\text{Na}_3\text{VO}_4$  thus further depletes total NEDD9::CasFAT. Despite low total NEDD9::CasFAT expression, the ratio of phosphorylated protein to total protein was significantly higher in the NEDD9::CasFAT-expressing cells (Fig. 7A). To determine whether tyrosine phosphorylation is rigidity dependent, phosphorylation was compared between cells grown on fibronectin-coated plastic versus fibronectin-coated 0.2 kPa gels (Fig. 7B). This revealed that phosphorylation increased with substrate rigidity (Fig. 7B).

NEDD9 phosphorylation has been reported to regulate the cleavage of the full-length NEDD9 protein, with de-phosphorylated NEDD9 cleaved to generate a 55 kDa N-terminal peptide (O'Neill and Golemis, 2001). Accordingly, there was significantly less cleavage product generated from the NEDD9::CasFAT protein versus wild-type NEDD9 (Fig. 7C). Moreover, stimulating increased tyrosine phosphorylation through pre-treatment with the phosphatase inhibitor  $\text{Na}_3\text{VO}_4$  reduces cleavage of both wild-type NEDD9 and NEDD9::FAKFAT (Fig. 7D). The role of cleavage in regulating cell migration was next tested by analysing cells that had been transfected with a NEDD9 expression construct in which the previously characterised DLVD cleavage site (Law et al., 1998,

2000) had been mutated to the sequence DLVA (NEDD9-DVLA), which abrogates the cleavage (Fig. 7E). As the NEDD9-DLVA mutant construct does not carry the mutations to prevent NEDD9 targeting by shRNA, analysis of this mutant was performed in NEDD9 $^{-/-}$  MEFs (Zhong et al., 2012). Providing independent confirmation of the role of CasFAT in A172 cells, expression of GFP–NEDD9::CasFAT also significantly reduced the speed of NEDD9 $^{-/-}$  MEFs compared to that upon expression of wild-type NEDD9 (Fig. 7F). Moreover, cells expressing the NEDD9-DLVA mutant protein also migrated significantly more slowly (Fig. 7F). In summary, the data suggest that NEDD9 cleavage is an important determinant of cell migration and, further, that CasFAT inhibits cleavage by inducing tyrosine phosphorylation.

## DISCUSSION

Numerous adhesion proteins express FAT domains, yet the role and function of the FAT domain remains poorly understood. In the present study, we show that the Cas-family FAT domains have both overlapping and distinct functions. Our data suggest that the FAT domain of p130Cas (referred to here as CasFAT) uniquely determines the mechanosensing function. The substitution of the CasFAT domain for the endogenous FAT

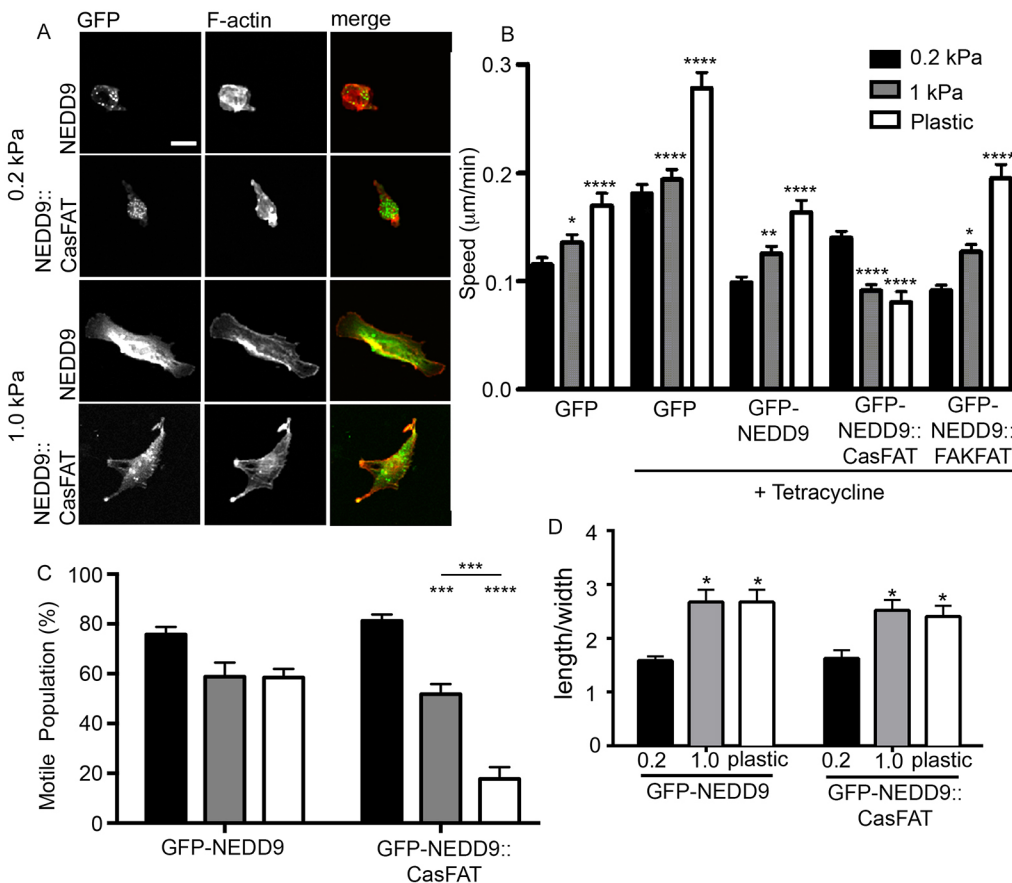


**Fig. 6. Rigidity-dependent cell speed.** (A) Confocal images of cells expressing the indicated GFP-tagged constructs, plated on fibronectin-coated polyacrylamide hydrogels of 0.2 kPa (top panels) and 1 kPa (bottom panels). Images show GFP (green), phalloidin staining of F-actin (red) and merged images. Scale bar: 20 µm. (B) Average speeds of control cells (Tet<sup>-</sup>) or following NEDD9 depletion (Tet<sup>+</sup>) and transfected with the indicated constructs. Cells were cultured on polyacrylamide hydrogels of 0.2 kPa (black bars), 1.0 kPa (grey bars) or plastic (white bars). Note that the cell speeds for plastic surfaces are the same as those represented in Fig. 5A, data are now plotted as a column graph. Error bars represent s.e.m. \* $P < 0.05$ , \*\* $P < 0.01$ , \*\*\* $P < 0.001$ , \*\*\*\* $P < 0.0001$ , one-way ANOVA with Tukey's multiple comparisons post-test. Data represent pooled means of  $n \geq 4$  independent experiments ( $\geq 155$  total cells analysed per construct). (C) Percentage of motile cells under the indicated conditions. Error bars represent s.e.m. \*\*\* $P < 0.001$ , \*\*\*\* $P < 0.0001$ , one-way ANOVA with Tukey's multiple comparisons post-test. Data represent pooled means of  $n \geq 4$  independent experiments ( $\geq 155$  total cells analysed per construct). \* $P > 0.05$ , one-way ANOVA with Tukey's multiple comparisons post-test. There was no significant difference in polarity between transfectants grown on matching substrates.

domain of NEDD9 resulted in high level phosphorylation of NEDD9, reduced cleavage and proportionally reduced cell migration speeds. Our study illustrates how otherwise structurally homologous protein domains can confer opposite cellular functions.

While a mechanosensing role for NEDD9 has been inferred in the past based on sequence and functional homology with p130Cas, to date this has not been experimentally validated. In the present study, we have analysed the consequence of NEDD9 expression for cell migration in response to substrates with a range of rigidities. We found increasing cell speed in response to more rigid substrates. Interestingly, NEDD9 depletion resulted in ~1.5-fold higher speeds overall, regardless of substrate rigidity. Collectively, these data suggest that, unlike p130Cas, NEDD9 may not have a mechanosensory function, at least in terms of regulating cell migration. In contrast, cells expressing NEDD9::CasFAT displayed an inverse relationship between substrate rigidity and cell speed, with the fastest cell speeds seen on the softest gels. Thus, in addition to previous data suggesting that the SH3 domain confers a mechanosensory function (Janoštiak et al.,

2014b), our data suggest an important role for CasFAT in mechanosensing.

Rigidity-mediated activation of p130Cas leads to phosphorylation of the p130Cas SD (Sawada et al., 2006), and our data reveal that substitution of the p130Cas FAT domain for that of NEDD9 similarly induces NEDD9 phosphorylation. The p130Cas Src-binding site diverges from the NEDD9 site as it is a bipartite binding motif, consisting of a polyproline Src SH3-binding domain juxtaposed to the Src SH2-binding domain (O'Neill et al., 2000). Although it has previously been shown that the p130Cas polyproline domain is required in order for Src to induce colony formation in soft agar when co-transfected with p130Cas (Huang et al., 2002), our data indicate that the polyproline domain may not be required for the p130Cas mechanosensing function. Interestingly, structural analysis of CasFAT suggests that it mediates tight binding to the interacting partner NSP3 by virtue of the bipartite binding motif (Mace et al., 2011).

We have previously shown that phosphorylation of the NEDD9 SD is a critical determinant of the rate of NEDD9 exchange at focal adhesions (Bradbury et al., 2014) and,

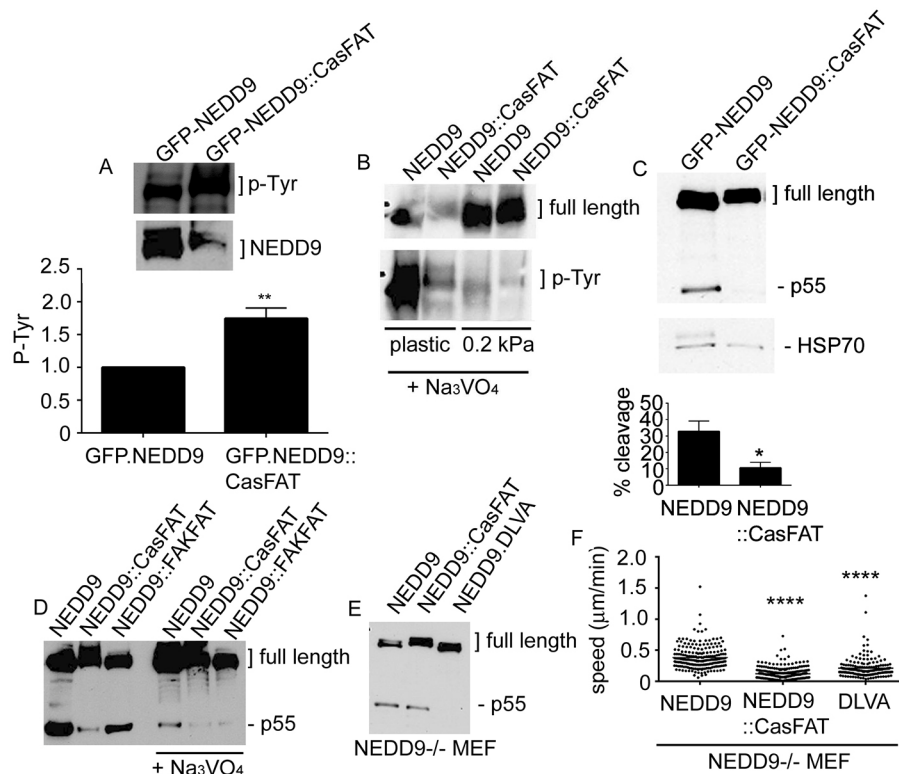


**Fig. 7. Rigidity-dependent regulation of phosphorylation, cleavage and migration.** (A) Western blot showing phosphorylation of tyrosine (p-Tyr) residues on exogenously expressed GFP–NEDD9 and GFP–NEDD9::CasFAT. Histogram underneath shows the levels of tyrosine phosphorylation expressed relative to the total GFP-tagged protein.  $**P < 0.01$ , Student's *t*-test. (B) Comparison of tyrosine phosphorylation of exogenous proteins extracted from cells grown on fibronectin-coated plastic versus fibronectin-coated 0.2 kPa gels. All cells were pre-treated with the tyrosine phosphatase inhibitor  $\text{Na}_3\text{VO}_4$ . Shown are the GFP-tagged full-length proteins and phosphorylated-tyrosine levels of the full length molecules. Blots were stripped subsequent to anti-phosphorylated-tyrosine analysis and then re-probed with anti-NEDD9 antibodies. (C) Expression of GFP-tagged full length proteins and the p55 NEDD9 N-terminal cleavage product (Fig. 1A shows location of the DLVD cleavage site). Note that the blots showing the NEDD9 cleavage product are the same as those in Fig. 2C but prior to HSP70 immunoblotting. Controls are from the subsequent HSP70 reprobe of the blot that is shown in Fig. 2C. The histogram underneath shows densitometry quantification of the percentage of cleavage  $[(p55/\text{full length} + p55) \times 100]$ . Analysis was performed on three independent biological replicates;  $*P < 0.05$ , Student's *t*-test. (D) Western blots of lysates from cells expressing the indicated exogenous proteins (all GFP tagged). Cells were treated under control conditions or with the phosphatase inhibitor  $\text{Na}_3\text{VO}_4$  as indicated. Expression of the NEDD9 p55 cleavage product is indicated. (E) Mutation of the DLVD cleavage site (position indicated in Fig. 1A) to DLVA abrogates production of the 55 kDa cleavage product. Western blot shows expression of the indicated exogenous GFP-tagged proteins expressed in NEDD9 $^{-/-}$  MEFs. (F) Speeds of individual NEDD9 $^{-/-}$  MEFs transfected with the indicated GFP-tagged expression constructs.  $****P < 0.0001$ , one-way ANOVA with Tukey's post-comparison test. Data shown are mean  $\pm$  s.e.m.

congruent with this finding, the CasFAT-containing NEDD9 protein with high levels of phosphorylation has significantly slower exchange rates at the focal adhesions. Phosphorylation of the p130Cas substrate domain conversely accelerates p130Cas displacement from focal adhesions and increases cell migration speed (Meenderink et al., 2010; Machiyama et al., 2014). Thus, these two highly related proteins employ the same mechanism – phosphorylation of the SD – to deliver opposite functional outcomes. It is notable that mutation of a single tyrosine residue that is conserved between NEDD9 and p130Cas and that forms a consensus binding site for the adaptor protein Crk also has opposite effects on cell migration outcomes (Baquiran et al., 2013). Previous studies have revealed that NEDD9 is post-translationally cleaved, releasing a 55 kDa N-terminal protein, and that this is regulated by phosphorylation (Law et al., 1998; O'Neill and Golemis, 2001). Data in the present study confirm that increased phosphorylation reduces cleavage and that abrogating cleavage inhibits cell migration.

Collectively, the data presented in this study highlight a specific role for the FAT domain of p130Cas in mechanosensing. Although FAK and vinculin are known to be involved in mechanosensing and

mechanotransduction (Janoštiak et al., 2014a; Goldmann, 2016), the specific roles of their FAT domains in this process is unknown. Notably, our study reveals that, unlike CasFAT, the FAT domain of FAK does not change migration speed. In future, it will be interesting to analyse the role of FAT domains in the mechanosensing and mechanotransduction properties of other proteins containing such domains.

## MATERIALS AND METHODS

### Sequence alignments

Sequence alignment of FAT domains, based on previously described structural analyses (Arold et al., 2002; Garron et al., 2009), was performed using PRALINE (<http://www.ibi.vu.nl/programs/pralinewww>) (Simossis and Heringa, 2005). The following sequences were compared: NEDD9 *Homo sapiens* (Q14511-1), *Mus musculus* (NM\_017464), *Rattus norvegicus* (NM\_001011922), *Gallus gallus* (XM\_418946); p130Cas *Homo sapiens* (P56941-1), *Mus musculus* (NM\_009954), *Rattus norvegicus* (NM\_012931), *Gallus gallus* (XM\_414057).

### cDNA expression constructs

The plasmids used include previously described expression constructs for GFP and GFP-tagged human NEDD9 (O'Neill and Golemis, 2001) and

GFP-tagged rat p130Cas. The GFP-tagged NEDD9 expression construct in which the NEDD9 FAT domain was exchanged for the p130Cas FAT domain was generated using overlap-extension PCR. The following primers were used to generate a NEDD9 sequence with the FAT domain deleted: forward, 5'-GGGGCGGGGGAATTCATGAAGTATAAGAATCTT-3'; reverse, 5'-CAGTTGACTTTTCCCTGGGGTAGGCTCTG-3'. The p130Cas FAT domain: forward, 5'-CAGAGCCTACCCAGGGAAAAAGTCAACTG-3'; reverse, 5'-ATTTCTCGAGTCATG CTGCTGCAAGTGTCC-3'. The two products were subsequently mixed and a new cDNA generated using the first forward primer and the final reverse primer. The resulting product was digested with EcoRI–XhoI and ligated with a similarly digested GFP-C4 vector DNA, creating the in-frame GFP–NEDD9::CasFAT expression construct. The same procedure was used to generate the GFP–NEDD9::FAKFAT construct, with the exception of the specific primer sequences. To generate a NEDD9 sequence with the FAT domain deleted, the same forward primer was used but the reverse primer sequence was 5'-ACTAATTTCTGGGGTTGGGGTAGGCTCTG-3'. The FAK FAT domain was generated using the following primers: forward, 5'-CTACCCCAACCCCAAGAAATTAGTCCACCT-3'; reverse, 5'-ATTTCTCGAGTCAGTGGGGTCTGTTTGTCCAAG-3'. All constructs were confirmed by DNA sequencing. NEDD9 shRNA-resistant cDNA expression constructs were generated by mutation of the shRNA recognition sequence (four silent point mutations at nucleotides 1536 (C to A), 1539 (G to C), 1542 (T to C) and 1545 (C to T)). Sequence mutagenesis was performed by GenScript (NJ, USA), and all sequences were independently verified by DNA sequencing.

### Antibodies

Primary antibodies used in the study [dilutions for western blot (WB) and immunofluorescence (IF) indicated in brackets] include antibodies to paxillin (clone 349; 610051) (IF: 1/1000 dilution) and p130Cas (clone 21; 610271) (WB: 1/1000 dilution) from BD Transduction Labs; FAK (clone D2R2E; 13009) (WB: 1/1000) and NEDD9 (clone 2G9; 4044) (WB: 1/1000) (Cell Signaling Technologies; phosphorylated tyrosine (clone 4G10; 05-321) (WB: 1:500) from Merck-Millipore (Darmstadt, Germany); HSP-70 (clone BRM-22; H5147) (WB: 1:3000) from Sigma Aldrich (Missouri, USA). Secondary antibodies used throughout this study were donkey anti-mouse Cy3, donkey anti-mouse Cy5, donkey anti-rabbit Cy3 from Molecular Probes (Life Technologies); sheep anti-mouse horseradish peroxidase (HRP)-conjugated and donkey anti-rabbit HRP-conjugated antibodies from GE Life Sciences.

### Cell lines

A172 glioblastoma cells were maintained in Dulbecco's modified eagle's medium (DMEM) supplemented with 10% foetal bovine serum (FBS). Before generating tetracycline-inducible NEDD9 knockdown A172 cells, the identity of the cells was independently verified by CellBank Australia. Inducible knockdown lines were created using the BLOCK-iT™ Inducible H1 RNAi Entry Vector Kit (Life Technologies) in conjunction with the BLOCK-iT™ Inducible H1 Lentiviral RNAi System (Life Technologies) as per the manufacturer's instructions. An shRNA targeting NEDD9 (NEDD9 shRNA) beginning at nucleotide 1529 (5'-CACCGCTGGTCCCTGAATATCTTGGCGAACCAAGATATTCAGGGACCAGC-3') was cloned into the pLenti4 backbone. Tetracycline-inducible NEDD9 shRNA cells were selected and maintained in DMEM supplemented with 10% FBS (v/v), 2 µg/ml blasticidin and 200 µg/ml zeocin, and passaged every third day at a ratio of 1:6. To induce NEDD9 knockdown, 1 µg/ml tetracycline was added to the medium, and cells were incubated for 72 h at 37°C under 5% CO<sub>2</sub>. NEDD9<sup>-/-</sup> mouse embryo fibroblasts have been previously described (Zhong et al., 2012).

### Protein extraction, immunoblotting and immunofluorescence

Phosphatase inhibitor pre-treatment was achieved by incubating cells with 500 µM of Na<sub>3</sub>VO<sub>4</sub> solution (prepared as described previously, Brown and Gordon, 1984) for 6 h. Cell monolayers were placed on ice and washed twice with cold PBS and extracted in the appropriate volume of PTY lysis buffer [50 mM HEPES (pH 7.5), 50 mM NaCl, 5 mM EDTA, 1% Triton

X-100 (v/v), 50 mM NaF, 10 mM Na<sub>4</sub>P<sub>2</sub>O<sub>7</sub>·10H<sub>2</sub>O]. Cells were collected with a cell scraper, and lysates were centrifuged at 15,500 g for 10 min at 4°C to remove non-solubilised proteins. The resulting supernatant was collected and the cell pellet discarded. Extracted proteins were loaded into wells of SDS-polyacrylamide gels of the appropriate acrylamide percentage. Separated proteins were then electro-transferred onto methanol-activated Immobilon PVDF transfer membrane (0.45 mm; Millipore) using chilled transfer buffer [0.05 M Tris, 0.04 M glycine, 20% methanol (v/v)]. Bound HRP-conjugated antibodies were detected using Western Lighting Chemiluminescence Reagent followed by exposure to X-ray film (Fujifilm, Australia), developed using an X-ray developer (Konica). For immunofluorescence, cells grown on glass slides were fixed in a 4% PFA in PBS solution (w/v) for 10 min and permeabilised [0.2% Triton X-100 (v/v), 0.5% BSA (w/v), PBS] for 15 min, followed by antibody probing and the addition of DAPI (1:10000) and fluorescently tagged phalloidin. Coverslips were mounted using FluoroSave (Calbiochem). Cells were imaged using an inverted confocal microscope (Leica SP5) equipped with a HCV PL APO CS 63×1.4 oil objective. Cell images were captured using the following settings: 512×512 pixels at 100 Hz with a line average of 8. For GFP-expressing cells, the argon laser power was set to 20% with the 488 nm laser set to an intensity of 20%, the smart gain and offset were set to 1100.0 V and 0.0%, respectively. For cells immunofluorescently labelled with Cy3- and Cy5-tagged secondary antibodies, the 561 nm and 633 nm lasers were set to 20% with a smart gain of 800 V and 1060 V, respectively, with both wavelengths having the offset at 0.0%. For nuclei excitation, the 405 nm laser was again set 20% with the smart gain set to 600 V.

### Polyacrylamide hydrogels

Easy-coat polyacrylamide (PAM) hydrogels of a defined Young's modulus (*E*) in 35-mm Petrisoft (plastic bottom) and Softview (glass bottom) cell culture dish formats were purchased (Matrigen, CA). Petrisoft dishes were used for brightfield-based assessment of migration and morphology experiments, and Softview dishes for confocal microscopy. PAM hydrogels were coated with fibronectin at room temperature for 1 h under sterile conditions and then used immediately. Cells were seeded onto gels at densities that yielded single non-touching cells.

### AFM and magnetic tweezers

To investigate the mechanical properties of the cells with AFM (MFP-3D, Asylum Research, CA), arrays of 20×20 force curves on a 20×20 (or 10×10) µm areas were recorded on the sample immersed in medium at 37°C in force spectroscopy mode. The microscope was mounted on an anti-vibration table (Herzan, CA) and operated within an acoustic isolation enclosure (TMC). First, the cells were localised using an integrated optical microscope. To reduce the influence of the cantilever edge, only regions of the cell that were at maximum height (furthest from the coverslip) were considered for analysis. The force curves were recorded using a SiNi cantilever (Budget Sensors, Bulgaria) having a nominal spring constant *K<sub>N</sub>*=0.06 N/m. Before use, the cantilevers were calibrated against a glass slide, and with the thermal vibration method. For all the experiments, the loading force was kept constant at 400 pN (indentation of about 300 nm) and the velocity at 2 µm/s. The force-indentation curves were analysed using IGOR software. The Young's modulus, *E*, was calculated using the Oliver–Pharr model. The Young's modulus determined from AFM measurements is a relative value and can only be used for comparative studies in cases when all the experimental conditions are kept the same. Magnetic tweezer experiments to measure adhesive force to fibronectin-coated beads was performed as previously described (Zhong et al., 2012).

### Adhesion assay

Cell adhesion assays were conducted as per the manufacturer's instructions (Cell Biolabs, CA, USA). Briefly, 7.5×10<sup>4</sup> cells were plated onto extracellular matrix-coated wells and incubated for 90 min at 37°C under 5% CO<sub>2</sub>. Medium was then removed and cells were washed with PBS. Cell Stain Solution was added and incubated for 10 min at room temperature. The cells were then washed with dH<sub>2</sub>O and allowed to air dry before the addition of Extraction Solution; cells were then incubated for 10 min at

room temperature with orbital shaking. Finally, the extracted samples were transferred to a 96 well plate and the optical density measured at 560 nm.

### Transfections

Transfections were performed using electroporation (Amaxa Nucleofector II, LONZA, Melbourne, Australia). A172 cells were transfected using the Cell Line Nucleofector Kit V according to the manufacturer's instructions. Briefly, the day before transfection, cells were re-plated to stimulate exponential growth. The following day,  $2 \times 10^6$  cells were collected and resuspended in Nucleofection Solution, 10  $\mu$ g of plasmid DNA was added and the mixture transferred to a glass cuvette. The cuvette was then placed in the electroporator and transfections carried out using the U-029 preset program. Following nucleofection, cells were resuspended in complete culture medium and plated at the indicated densities for further experiments.

### Time-lapse imaging and cell tracking

The day prior to imaging,  $8 \times 10^4$  cells were seeded into either a single well of a 6-well plate (Corning) or 35-mm dishes containing PAM hydrogels and incubated overnight at 37°C under 5% CO<sub>2</sub>. All dishes were first coated with 2  $\mu$ g/cm<sup>2</sup> of fibronectin. The following day, complete medium was replaced with CO<sub>2</sub>-independent medium and equilibrated for an hour at 37°C. Migration studies were conducted over a 12 h period with frames taken every 5 min. Cells were imaged using a 20 $\times$  air objective of an automated Olympus IX81 inverted microscope controlled by Metamorph v6.3 software (Molecular Devices) and equipped with a heating chamber and floating anti-vibration table. GFP-positive cells were first identified in fluorescent mode and subsequently tracked throughout the time course in the brightfield view (12 h). Cells undergoing division or apoptosis were excluded from image analysis. Cell speeds were calculated from the MSD of the nucleus position versus time. The percentage of moving cells was determined as previously reported (Grundy et al., 2016).

### Acknowledgements

The authors acknowledge Dr Lawrence Cantrill for microscopy assistance, and Dr Lena Lautscham, Dr Navid Bonakdar, Achim Schilling and Astrid Mainka for their assistance in conducting the magnetic tweezer assay.

### Competing interests

The authors declare no competing or financial interests.

### Author contributions

P.M.B., K.T., C.M., K.R.G., L.L., R.D., S.M. and E.T. were involved in experimental work and data analysis. P.M.B., B.F., J.C.-W. and G.M.O. were involved in project planning and data analysis. P.M.B. and G.M.O. wrote the manuscript.

### Funding

This work was supported by the New South Wales Cancer Council (Cancer Council NSW) (RG12/06 to G.M.O. and B.F.), a University of Sydney Strategic Priority Areas for Collaboration Grant and generous funding through Dooley's Lidcombe Catholic Club. P.M.B. holds a University of Sydney postgraduate student scholarship and received a German Academic Exchange Service award (Deutscher Akademischer Austauschdienst). C.M. was supported by a C4-fellowship from the Kids Cancer Project.

### References

Arold, S. T., Hoellerer, M. K. and Noble, M. E. M. (2002). The structural basis of localization and signaling by the focal adhesion targeting domain. *Structure* **10**, 319–327.

Bae, Y. H., Mui, K. L., Hsu, B. Y., Liu, S.-L., Cretu, A., Razinia, Z., Xu, T., Pure, E. and Assoian, R. K. (2014). A FAK-Cas-Rac-lamellipodin signaling module transduces extracellular matrix stiffness into mechanosensitive cell cycling. *Sci. Signal.* **7**, ra57.

Baquiran, J. B., Bradbury, P. and O'Neill, G. M. (2013). Tyrosine Y189 in the substrate domain of the adhesion docking protein NEDD9 is conserved with p130Cas Y253 and regulates NEDD9-mediated migration and focal adhesion dynamics. *PLoS One* **8**, e69304.

Bradbury, P., Bach, C. T., Paul, A. and O'Neill, G. M. (2014). Src kinase determines the dynamic exchange of the docking protein NEDD9 (neural precursor cell expressed developmentally down-regulated gene 9) at focal adhesions. *J. Biol. Chem.* **289**, 24792–24800.

Bradshaw, L. N., Zhong, J., Bradbury, P., Mahmassani, M., Smith, J. L., Ammit, A. J. and O'Neill, G. M. (2011). Estradiol stabilizes the 105-kDa phospho-form of

the adhesion docking protein NEDD9 and suppresses NEDD9-dependent cell spreading in breast cancer cells. *Biochim. Biophys. Acta* **1813**, 340–345.

Brami-Cherrier, K., Gervasi, N., Arsenieva, D., Walkiewicz, K., Boutterin, M.-C., Ortega, A., Leonard, P. G., Seantier, B., Gasmi, L., Bouceba, T. et al. (2014). FAK dimerization controls its kinase-dependent functions at focal adhesions. *EMBO J.* **33**, 356–370.

Brown, D. J. and Gordon, J. A. (1984). The stimulation of pp60v-src kinase activity by vanadate in intact cells accompanies a new phosphorylation state of the enzyme. *J. Biol. Chem.* **259**, 9580–9586.

Bui, L.-C., Tomkiewicz, C., Chevallier, A., Pierre, S., Bats, A.-S., Mota, S., Raingeaud, J., Pierre, J., Diry, M., Transy, C. et al. (2009). Nedd9/Hef1/Cas-L mediates the effects of environmental pollutants on cell migration and plasticity. *Oncogene* **28**, 3642–3651.

Cary, L. A., Han, D. C., Polte, T. R., Hanks, S. K. and Guan, J.-L. (1998). Identification of p130Cas as a mediator of focal adhesion kinase- promoted cell migration. *J. Cell Biol.* **140**, 211–221.

Donato, D. M., Ryzhova, L. M., Meenderink, L. M., Kaverina, I. and Hanks, S. K. (2010). Dynamics and mechanism of p130Cas localization to focal adhesions. *J. Biol. Chem.* **285**, 20769–20779.

Draheim, K. M., Li, X., Zhang, R., Fisher, O. S., Villari, G., Boggon, T. J. and Calderwood, D. A. (2015). CCM2-CCM3 interaction stabilizes their protein expression and permits endothelial network formation. *J. Cell Biol.* **208**, 987–1001.

Fashena, S. J., Einarson, M. B., O'Neill, G. M., Patriotis, C. and Golemis, E. A. (2002). Dissection of HEF1-dependent functions in motility and transcriptional regulation. *J. Cell Sci.* **115**, 99–111.

Garron, M.-L., Arsenieva, D., Zhong, J., Bloom, A. B., Lerner, A., O'Neill, G. M. and Arold, S. T. (2009). Structural insights into the association between BCAR3 and Cas family members, an atypical complex implicated in anti-oestrogen resistance. *J. Mol. Biol.* **386**, 190–203.

Goldmann, W. H. (2016). Role of vinculin in cellular mechanotransduction. *Cell Biol. Int.* **40**, 241–256.

Grundy, T. J., De Leon, E., Griffin, K. R., Stringer, B. W., Day, B. W., Fabry, B., Cooper-White, J. and O'Neill, G. M. (2016). Differential response of patient-derived primary glioblastoma cells to environmental stiffness. *Sci. Rep.* **6**, 23353.

Harte, M. T., Hildebrand, J. D., Burnham, M. R., Bouton, A. H. and Parsons, J. T. (1996). p130Cas, a substrate associated with v-Src and v-Crk, localizes to focal adhesions and binds to focal adhesion kinase. *J. Biol. Chem.* **271**, 13649–13655.

Hayashi, I., Vuori, K. and Liddington, R. C. (2002). The focal adhesion targeting (FAT) region of focal adhesion kinase is a four-helix bundle that binds paxillin. *Nat. Struct. Biol.* **9**, 101–106.

Hoellerer, M. K., Noble, M. E. M., Labesse, G., Campbell, I. D., Werner, J. M. and Arold, S. T. (2003). Molecular recognition of paxillin LD motifs by the focal adhesion targeting domain. *Structure* **11**, 1207–1217.

Huang, J., Hamasaki, H., Nakamoto, T., Honda, H., Hirai, H., Saito, M., Takato, T. and Sakai, R. (2002). Differential regulation of cell migration, actin stress fiber organization, and cell transformation by functional domains of Crk-associated substrate. *J. Biol. Chem.* **277**, 27265–27272.

Izumchenko, E., Singh, M. K., Plotnikova, O. V., Tikhmyanova, N., Little, J. L., Serebriskii, I. G., Seo, S., Kurokawa, M., Egleston, B. L., Klein-Szanto, A. et al. (2009). NEDD9 promotes oncogenic signaling in mammary tumor development. *Cancer Res.* **69**, 7198–7206.

Janoštiak, R., Pataki, A. C., Brábek, J. and Rösel, D. (2014a). Mechanosensors in integrin signaling: the emerging role of p130Cas. *Eur. J. Cell Biol.* **93**, 445–454.

Janoštiak, R., Brábek, J., Auernheimer, V., Tatárová, Z., Lautscham, L. A., Dey, T., Gemperle, J., Merkel, R., Goldmann, W. H., Fabry, B. et al. (2014b). CAS directly interacts with vinculin to control mechanosensing and focal adhesion dynamics. *Cell. Mol. Life Sci.* **71**, 727–744.

Kim, M., Gans, J. D., Nogueira, C., Wang, A., Paik, J.-H., Feng, B., Brennan, C., Hahn, W. C., Cordon-Cardo, C., Wagner, S. N. et al. (2006). Comparative oncogenomics identifies NEDD9 as a melanoma metastasis gene. *Cell* **125**, 1269–1281.

Klemke, R. L., Leng, J., Molander, R., Brooks, P. C., Vuori, K. and Cheresch, D. A. (1998). CAS/Crk coupling serves as a "molecular switch" for induction of cell migration. *J. Cell Biol.* **140**, 961–972.

Kong, C., Wang, C., Wang, L., Ma, M., Niu, C., Sun, X., Du, J., Dong, Z., Zhu, S., Lu, J. et al. (2011). NEDD9 is a positive regulator of epithelial-mesenchymal transition and promotes invasion in aggressive breast cancer. *PLoS ONE* **6**, e22666.

Law, S. F., Zhang, Y.-Z., Klein-Szanto, A. J. P. and Golemis, E. A. (1998). Cell cycle-regulated processing of HEF1 to multiple protein forms differentially targeted to multiple subcellular compartments. *Mol. Cell Biol.* **18**, 3540–3551.

Law, S. F., O'Neill, G. M., Fashena, S. J., Einarson, M. B. and Golemis, E. A. (2000). The docking protein HEF1 is an apoptotic mediator at focal adhesion sites. *Mol. Cell Biol.* **20**, 5184–5195.

Li, X., Zhang, R., Zhang, H., He, Y., Ji, W., Min, W. and Boggon, T. J. (2010). Crystal structure of CCM3, a cerebral cavernous malformation protein critical for vascular integrity. *J. Biol. Chem.* **285**, 24099–24107.

Liu, X., Elia, A. E., Law, S. F., Golemis, E. A., Farley, J. and Wang, T. (2000). A novel ability of Smad3 to regulate proteasomal degradation of a Cas family member HEF1. *EMBO J.* **19**, 6759–6769.

- Lucas, J. T., Jr, Salimath, B. P., Slomiany, M. G. and Rosenzweig, S. A. (2010). Regulation of invasive behavior by vascular endothelial growth factor is HEF1-dependent. *Oncogene* **29**, 4449-4459.
- Mace, P. D., Wallez, Y., Dobaczewska, M. K., Lee, J. E. J., Robinson, H., Pasquale, E. B. and Riedl, S. J. (2011). NSP-Cas protein structures reveal a promiscuous interaction module in cell signaling. *Nat. Struct. Mol. Biol.* **18**, 1381-1387.
- Machiyama, H., Hirata, H., Loh, X. K., Kanchi, M. M., Fujita, H., Tan, S. H., Kawauchi, K. and Sawada, Y. (2014). Displacement of p130Cas from focal adhesions links actomyosin contraction to cell migration. *J. Cell Sci.* **127**, 3440-3450.
- Meenderink, L. M., Ryzhova, L. M., Donato, D. M., Gochberg, D. F., Kaverina, I. and Hanks, S. K. (2010). P130Cas Src-binding and substrate domains have distinct roles in sustaining focal adhesion disassembly and promoting cell migration. *PLoS ONE* **5**, e13412.
- Mui, K. L., Bae, Y. H., Gao, L., Liu, S. L., Xu, T., Radice, G. L., Chen, C. S. and Assoian, R. K. (2015). N-cadherin induction by ECM stiffness and FAK overrides the spreading requirement for proliferation of vascular smooth muscle cells. *Cell Rep.* **10**, 1477-1486.
- Nakamoto, T., Sakai, R., Honda, H., Ogawa, S., Ueno, H., Suzuki, T., Aizawa, S., Yazaki, Y. and Hirai, H. (1997). Requirements for localization of p130Cas to focal adhesions. *Mol. Cell Biol.* **17**, 3884-3897.
- Natarajan, M., Stewart, J. E., Golemis, E. A., Pugacheva, E. N., Alexandropoulos, K., Cox, B. D., Wang, W., Grammer, J. R. and Gladson, C. L. (2006). HEF1 is a necessary and specific downstream effector of FAK that promotes the migration of glioblastoma cells. *Oncogene* **25**, 1721-1732.
- Ohashi, Y., Tachibana, K., Kamiguchi, K., Fujita, H. and Morimoto, C. (1998). T cell receptor-mediated tyrosine phosphorylation of Cas-L, a 105-kDa Crk-associated substrate-related protein, and its association of Crk and C3G. *J. Biol. Chem.* **273**, 6446-6451.
- O'Neill, G. M. and Golemis, E. A. (2001). Proteolysis of the docking protein HEF1 and implications for focal adhesion dynamics. *Mol. Cell Biol.* **21**, 5094-5108.
- O'Neill, G. M., Fashena, S. J. and Golemis, E. A. (2000). Integrin signalling: a new Cas(t) of characters enters the stage. *Trends Cell Biol.* **10**, 111-119.
- Ruest, P. J., Shin, N.-Y., Polte, T. R., Zhang, X. and Hanks, S. K. (2001). Mechanisms of CAS substrate domain tyrosine phosphorylation by FAK and Src. *Mol. Cell Biol.* **21**, 7641-7652.
- Sawada, Y., Tamada, M., Dubin-Thaler, B. J., Cherniavskaya, O., Sakai, R., Tanaka, S. and Sheetz, M. P. (2006). Force sensing by mechanical extension of the Src family kinase substrate p130Cas. *Cell* **127**, 1015-1026.
- Schmalzigaug, R., Garron, M.-L., Roseman, J. T., Xing, Y., Davidson, C. E., Arold, S. T. and Premont, R. T. (2007). GIT1 utilizes a focal adhesion targeting-homology domain to bind paxillin. *Cell. Signal.* **19**, 1733-1744.
- Seo, S., Nakamoto, T., Takeshita, M., Lu, J., Sato, T., Suzuki, T., Kamikubo, Y., Ichikawa, M., Noda, M., Ogawa, S. et al. (2011). Crk-associated substrate lymphocyte type regulates myeloid cell motility and suppresses the progression of leukemia induced by p210Bcr/Abl. *Cancer Sci.* **102**, 2109-2117.
- Simossis, V. A. and Heringa, J. (2005). PRALINE: a multiple sequence alignment toolbox that integrates homology-extended and secondary structure information. *Nucleic Acids Res.* **33**, W289-W294.
- Simpson, K. J., Selfors, L. M., Bui, J., Reynolds, A., Leake, D., Khvorova, A. and Brugge, J. S. (2008). Identification of genes that regulate epithelial cell migration using an siRNA screening approach. *Nat. Cell Biol.* **10**, 1027-1038.
- Singh, M. K., Dadke, D., Nicolas, E., Serebriiskii, I. G., Apostolou, S., Canutescu, A., Egleston, B. L. and Golemis, E. A. (2008). A novel cas family member, HEPL, regulates FAK and cell spreading. *Mol. Biol. Cell* **19**, 1627-1636.
- Tikhmyanova, N., Little, J. L. and Golemis, E. A. (2010). CAS proteins in normal and pathological cell growth control. *Cell. Mol. Life Sci.* **67**, 1025-1048.
- van Seventer, G. A., Salmen, H. J., Law, S. F., O'Neill, G. M., Mullen, M. M., Franz, A. M., Kanner, S. B., Golemis, E. A. and van Seventer, J. M. (2001). Focal adhesion kinase regulates beta1 integrin-dependent T cell migration through an HEF1 effector pathway. *Eur. J. Immunol.* **31**, 1417-1427.
- Zhong, J., Baquiran, J. B., Bonakdar, N., Lees, J., Ching, Y. W., Pugacheva, E., Fabry, B. and O'Neill, G. M. (2012). NEDD9 stabilizes focal adhesions, increases binding to the extra-cellular matrix and differentially effects 2D versus 3D cell migration. *PLoS ONE* **7**, e35058.